 doi:10.20944/preprints202107.0630.v1

Article

Hydrological responses to land use land cover change in the Fincha'a watershed, Ethiopia

Urgessa Kenea[1], Dereje Adeba[1], Motuma Shiferaw Regasa[2], and Michael Nones [2,*]

[1] Department of Hydraulic and Water Resources Engineering, Institute of Engineering and Technology, Wollega University, Ethiopia; keneaurgessa@gmail.com, mo_dereje2018@yahoo.com
[2] Department of Hydrology and Hydrodynamics, Institute of Geophysics Polish Academy of Sciences, Poland; mregasa@igf.edu.pl; mnones@igf.edu.pl
* Correspondence: mnones@igf.edu.pl

Abstract: Land use land cover (LULC) changes are highly pronounced in African countries, as they are characterized by an agriculture-based economy and a rapidly growing population. Understanding how land use/cover change (LULCC) influence watershed hydrology will enable local governments and policymakers to formulate and implement effective and appropriate response strategies to minimize the undesirable effects of future land use/cover change or modification and sustain the local socio-economic situation. The hydrological response of the Ethiopia Fincha'a watershed to LULCC happened during the last 30 years was investigated comparing the situation in three reference years: 1994, 2004 and 2018. The information was derived from Landsat sensors, respectively Landsat 5 TM, Landsat 7 ETM and Landsat 8 OLI/TIRS. The various LULC classes were derived via ArcGIS using a supervised classification system, and the accuracy assessment was done using confusion matrixes. For all the years investigated the overall accuracies and the kappa coefficients were higher than 80%, with 2018 as the more accurate year. The analysis of LULCC revealed that forest decreased by 19.99% between the years 1994-2004, and it decreased by 11.85% in the following period 2004-2018. Such decline in areas covered by forest is correlated to an expansion of cultivated land by 16.4% and 10.81%, respectively. After having evaluated the LULCC at the basin scale, the watershed was divided into 18 sub-watersheds, which contained 176 Hydrologic Response Units (HRUs), having a specific LULC. Accounting for such a detailed subdivision of the Fincha'a watershed, the SWAT model was firstly calibrated and validated on past data, and then applied to infer information on the hydrological response of each HRU on LULCC. The modelling results pointed out a general increase of average water flow, both during dry and wet periods, as a consequence of a shift of land coverage from forest and grass towards settlements and build-up areas. The present analysis pointed out the need of accounting for past and future LULCC in modelling the hydrological responses of rivers at the watershed scale.

Keywords: Africa; Ethiopia; Landsat; Land Use Land Cover Change; Remote Sensing; SWAT model

1. Introduction

Hydrological modelling and water resource management are highly related to the processes of the hydrologic cycle. This cycle can be affected by land use and land cover change. Land use and land cover (LULC) is an essential component of the terrestrial ecosystem, influencing various fundamental characteristics and processes such as the hydrological cycle, geomorphologic processes, land productivity and flora and fauna species [1]. Changes in LULC can have both short-term and long-lasting impacts on terrestrial hydrology, altering, for example, the long-term balance between rainfall and evapotranspiration and the resultant runoff [2]. Evaluating the past land use, types of changes and the forces behind them is paramount to understand the interrelationships between humans and the natural environment [3-4].

 doi:10.20944/preprints202107.0630.v1

Land use land cover changes (LULCC) are highly pronounced in developing countries, which are characterized by agriculture-based economics and rapidly increasing populations [5]. In those countries, the impact of LULC on biodiversity and human life is clear [6], as well as the need for better evaluating future trends and management strategies. In this sense, assessing the impacts of LULC changes on hydrology remains an important step in watershed management strategies inclusive of water resources planning and conservation measures. In their work, Meyer and Turner [7] discussed that land cover changes are caused by many natural and human driving forces. While the effects of natural causes like climate change are recognizable over a long period, the effects of human activities are generally more immediate. Population growth causes the degradation of resources that rely on the available land and the interactions between them are very complex and hard to be modelled. Interactions can make positive or negative effects on the resources. People demand land for food production as well as for housing, and in African countries is a common practice to clear the forest to make farming area and housing. The result of such a practice is that land cover and land use can vary at a quasi-daily scale, following human interventions.

The degree of modification of the natural land cover by human influences, the intensity of the changes, and the location of the land use within a catchment affect the extent to which the land use determines the hydrological response of a catchment. However, generally, these modifications are evaluated only at the local scale [8], involving difficulties in estimating the contribution of LULCC on the basin-wide hydrological cycle. To overcome such problems, hydrological modelling can be implied. Physically-based hydrological models simulate the spatially distributed streamflow time series, and so they can be used to estimate the relative contributions of land cover changes and climate change/variability at the daily, monthly or even annual time scale [9]. The Soil & Water Assessment Tool (SWAT) model has been reported to be a useful model for evaluating the effects of LULUC on the hydrological cycle, and it has been widely accepted as a cost-effective tool because of its advanced model configuration and numerous function, such as modelling limited data regions and evaluating various scenarios and agriculture management practices [10-11].

The sustainable use of water is becoming increasingly important in the legislative agenda of Ethiopia, as this is one of the developing countries from the world where agriculture is the backbone of the economy, and where agriculture is facing major environmental challenges associated with LULCC [6]. The overall goal of the Ethiopian Water Resource Policy is to enhance and promote all national efforts towards the efficient, equitable and optimum utilization of the available water resources of the country for significant socio-economic development on a sustainable basis. Therefore, a better understanding of how land use/cover change influences watershed hydrology will enable local governments and policymakers to formulate and implement effective and appropriate response strategies to minimize the undesirable effects of future land use/cover change or modification. In Ethiopia, changes in LULC are also playing a significant role in changing the natural hydrological processes, shifting them towards an increase in surface runoff volumes, an increase in evapotranspiration and a reduction of infiltration and consequent groundwater recharge [8,14]. Catching the dynamics of LULC and addressing how they affect the local livelihood is therefore paramount for establishing a sustainable development policy [15].

Using the Fincha'a watershed as a case study, the present work i) review past LULC, using three reference years (1994, 2008, 2018), ii) investigate the effects of LULCC on watershed hydrology. The first point was addressed via a combination of satellite imagery and Geographical Information Systems. Landsat images of the three years were classified using a supervised method, and then the various LULC were compared to derive past trends. After an adequate calibration and validation process. The SWAT model version 2012 was here used to evaluate the effect of LULCC on the Fincha'a basin hydrology, pointing out an increase of water discharge due to the loss of forest and grass areas in favour of agricultural and build-up zones.

Preprints (www.preprints.org) | NOT PEER-REVIEWED | Posted: 28 July 2021 doi:10.20944/preprints202107.0630.v1

2. Materials and Methods

2.1. Study area

The Fincha'a watershed is part of the Blue Nile basin and is located in the Oromia region, Horro Guduru Wollega zone, Ethiopia, between 9º10‟ 30" to 9º 46‟45" north latitude and between 37º 03‟ 00" to 37º 28‟ 30" east longitude (Figure 1). The watershed is bounded on the south by the Great Gibe River basin, on the north by the Abbay (Blue Nile) River basin, on the west by the Didessa sub-basin, and on the east by the Guder sub-basin. It covers an area of about 3,781 km^2, containing three sub-basins, namely the Fincha'a, Amerti and Neshe. It covers seven aanaa's (the Ethiopian second-lowest administrative unit): Abay Chomen, Guduru, Hababo Guduru, Jimma Rare, Horro, Jima Geneti and Jarte Jardega.

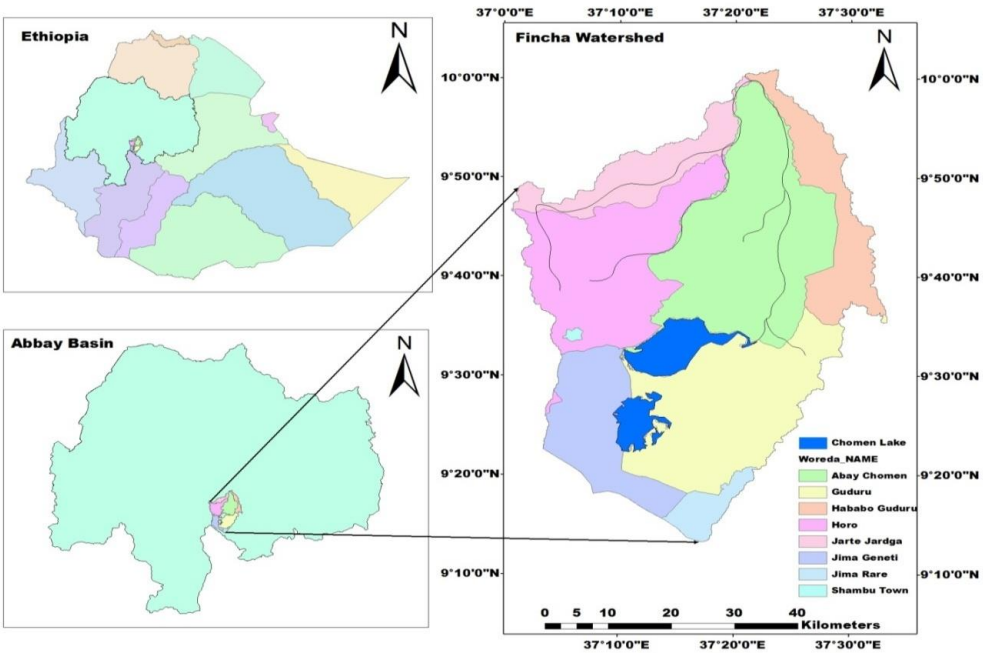

Figure 1. Location of the Fincha'a watershed within Ethiopia.

The study followed the workflow presented in Figure 2, and described in detail in the following sections.

Preprints (www.preprints.org) | NOT PEER-REVIEWED | Posted: 28 July 2021 doi:10.20944/preprints202107.0630.v1

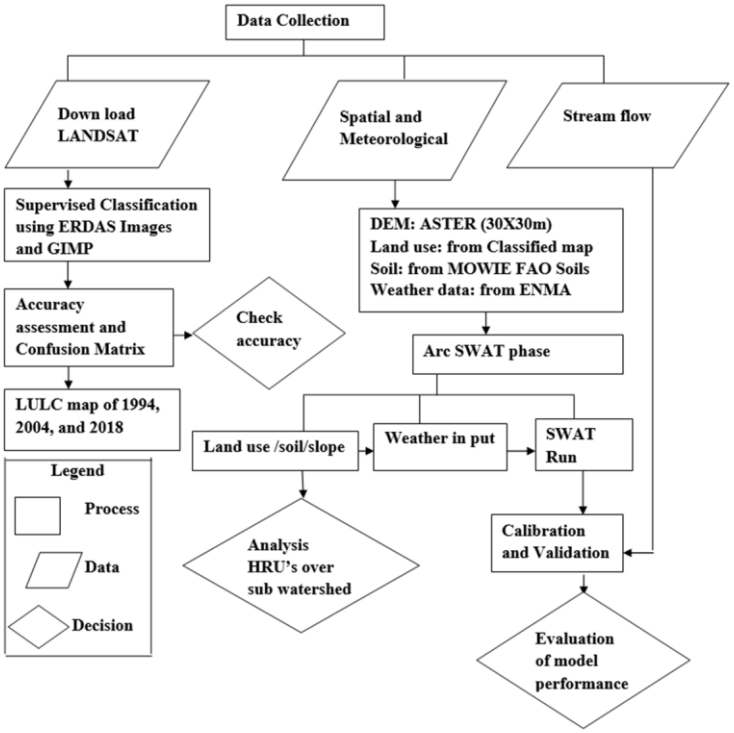

Figure 2. Conceptual framework of the study.

2.1.1 Watershed topography and geology

The altitude in the Fincha'a basin ranges approximately between 880 and 3200 m asl. The highlands in the western and southern part of the basin are higher in altitude, greater than 2200 m up to 3200 m asl. The lowlands have a lower altitude, less than 1400 m asl, and are located in the northern part.

The dominant soils of the area are clay, loam, and clay-loam, while a small part of the watershed in the northeastern part consists of Adigrat sandstone formation (Figure 3). The higher parts of the watershed near the boundary (where the drainage of all the streams begin) as well as the elevated parts in the middle of the watershed, which are isolated outcrops, are made of Quaternary volcanic [8].

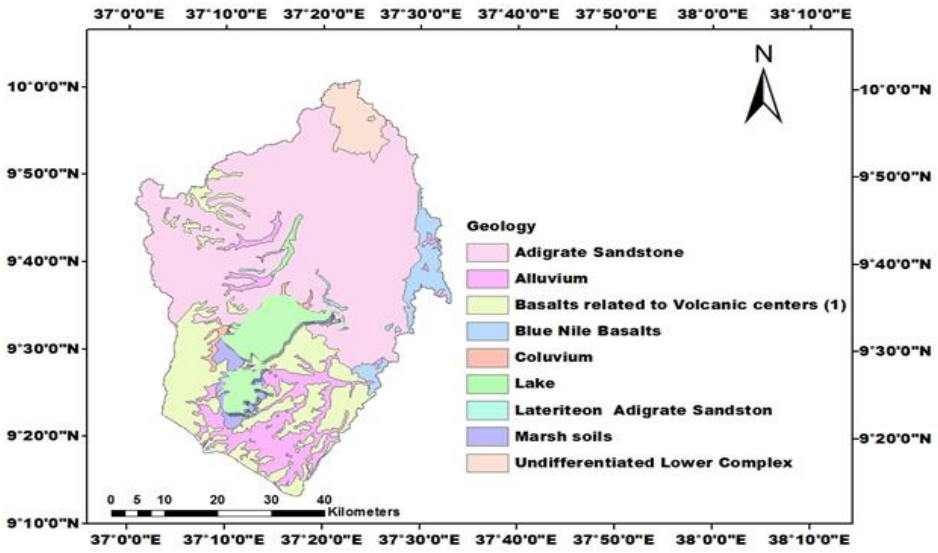

Figure 3. Geological map of the Fincha'a watershed (source: Abbay Basin Authority).

Preprints (www.preprints.org) | NOT PEER-REVIEWED | Posted: 28 July 2021 doi:10.20944/preprints202107.0630.v1

The Fincha'a reservoir would be in the Chomen swamp, the basin of which is covered with black clay of unknown depth. It may be as much as 10 meters deep and is believed to be underlain by volcanic rock. The soil cover forms an excellent impermeable blanket, therefore seepage is not considered to be a serious factor in this area.

2.1.2 Weather Data

The weather data were collected from Ethiopian National Metrological Agency (ENMA). Specifically, for the study period, daily data of maximum and minimum temperature, precipitation, relative humidity, wind and solar radiation were collected, referring to four gauging stations: Fincha'a, Homi, Shambu, and Neshe (Figure 4 and Table 2). All the data were combined and prepared to be used as input data for the SWAT model.

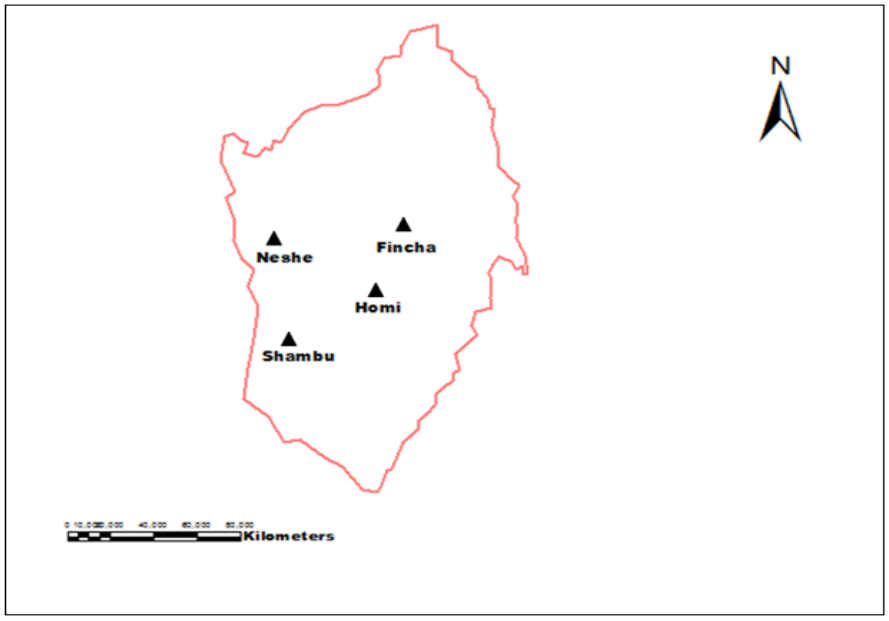

Figure 4. Location of the meteorological stations in the Fincha'a watershed.

Table 1. Meteorological stations of the Fincha'a watershed.

Name	**Year of record**	**X**	**Y**	**Elevation** [m asl]
Fincha'a	1989-2018	9.57	37.37	2248
Homi	1987-2018	9.621	37.241	2371
Shambu	1981-2018	9.5712	37.1	2460
Neshe	1981-2018	9.723	37.268	2060

Figure 5 summarizes the monthly values of rainfall and temperature in the Fincha'a watershed averaged over the study period. Details on the various parameters are provided in the following subsections.

Preprints (www.preprints.org) | NOT PEER-REVIEWED | Posted: 28 July 2021 doi:10.20944/preprints202107.0630.v1

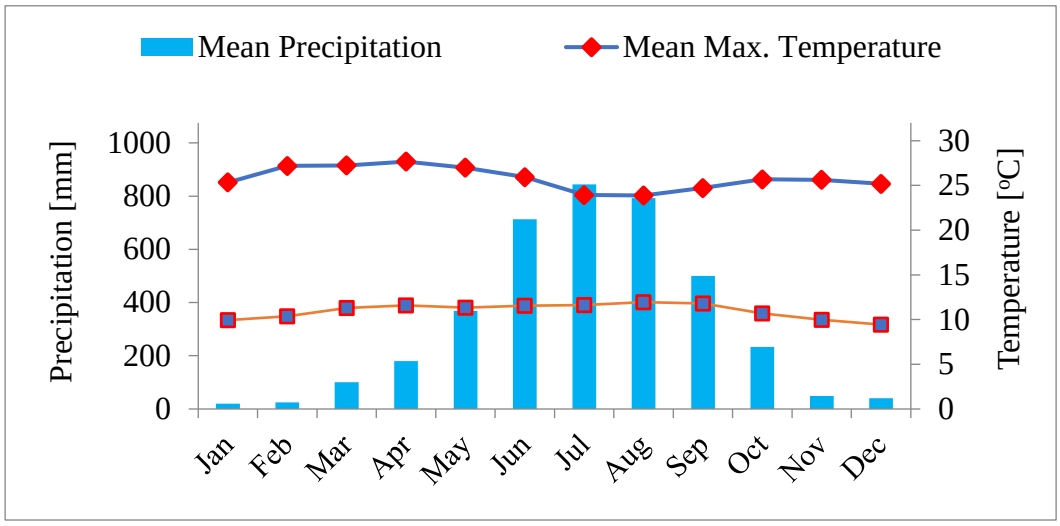

Figure 5. Average rainfall, minimum and maximum temperature in the Fincha'a watershed.

The daily flow data are required for calibrating the SWAT simulations. This data was obtained from the Ministry of Water, Irrigation, and Energy Office, and post-processed as per the requirement of the modelling tool. The calibration and validation were done on a daily and monthly basis, using the periods 1997-2004 for the calibration and 2005-2008 for validation. Missing and no-data were excluded from this process.

2.1.3 Temperature

The annual minimum and maximum temperatures of the watershed vary from 6.0 to 16.0°C and from 19.5 to 31.5 °C, respectively, (Figure 6), and are the lowest during summer, due to the prevailing cloud cover experienced during this season. The temperature is higher at the Homi metrological gauging station, where a maximum of 27.91°C was reached during the observed period, while the minimum temperature of 10.41°C was measured at the Fincha'a metrological gauging station.

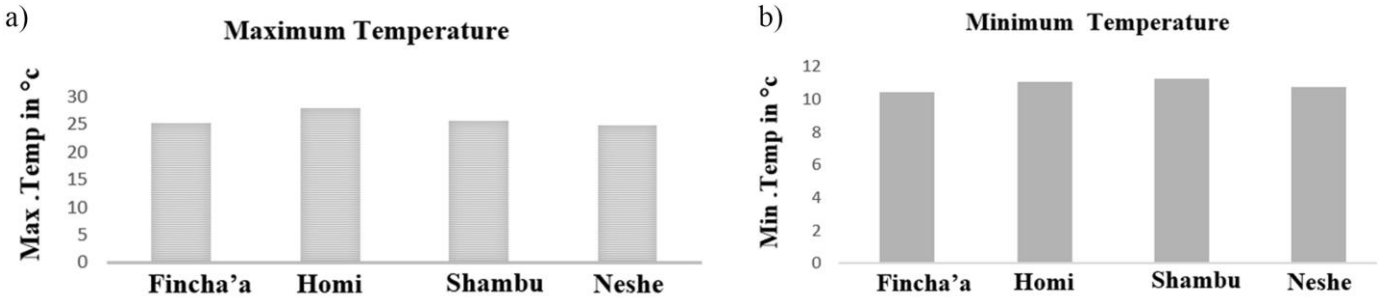

Figure 6. Maximum (left panel) and minimum (right panel) temperatures measured in the four stations.

2.1.4 Rainfall

The rainfall data collected from the stations may vary in their qualities and consistencies of record. There are five weather stations in the Fincha'a watershed, but the Hareto station was not used due to the short time record of weather data. The collected data have missing values in all the stations. The missing values in all stations were assigned with no data code (-99) which was then filled by the weather generator embodied in the SWAT model from the monthly weather parameter.

Preprints (www.preprints.org) | NOT PEER-REVIEWED | Posted: 28 July 2021 doi:10.20944/preprints202107.0630.v1

The watershed has an annual rainfall ranging between 960 mm and 1835 mm (Figure 7). Lower annual rainfall less than 1100 mm is observed in the northern lowlands of the sub-basin and higher rainfall greater than 1300 mm in the western and southern highlands. The rainfall presents a peak during the summer (July to August) and exhibits minimum values during the winter (December to February).

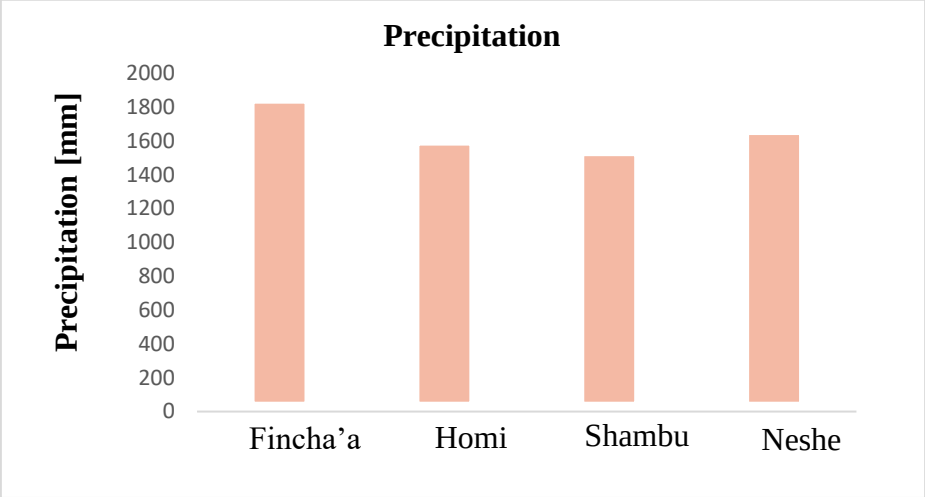

Figure 7. Annual precipitation measured in the four stations.

The double mass curve technique was used to check whether the collected rainfall data from Fincha'a sub-basin meteorological station were consistent through the selected period of study and checked whether corrections were needed or not. A group of certain numbers of neighbouring stations was chosen as base stations from the vicinity of a doubtful station and said as a doubtful station until it is checked. The precipitation of station x (doubtful station) can be corrected using eq. (1):

$$P_{cx} = P_x \frac{M_c}{M_a} \quad (1)$$

where P_{cx} represents the corrected precipitation at any period t at station X, while P_x is the corresponding original recorded precipitation, and M_c and M_a are the corrected and original slope of the double mass curve, respectively.

A Double Mass Curve was used to investigate whether there was inconsistency for the four considered gauging stations. The records of these stations did not indicate inconsistency, as the graph was found to follow a nearly straight line (Figure 8). This means that all the stations' data in the Fincha'a watershed were almost consistent.

Preprints (www.preprints.org) | NOT PEER-REVIEWED | Posted: 28 July 2021 doi:10.20944/preprints202107.0630.v1

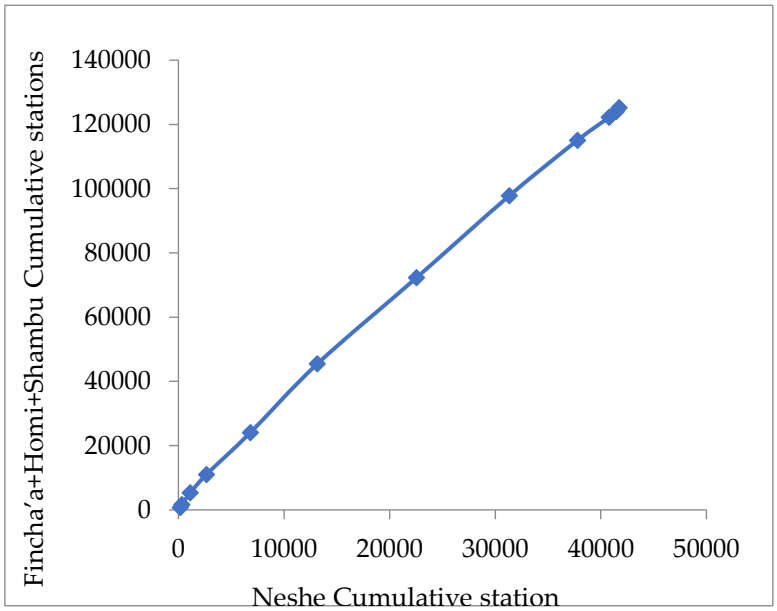

Figure 8. Double Mass Curve of the daily annual precipitation.

2.1.5 Evaporation

The potential evapotranspiration (PET) in the basin is generally between 1365 mm and 1970 mm per year. In the lowlands a higher temperature is generally observed, driving the PET to values higher than 1800 mm/yr. The highlands in the western and eastern parts of the basin show a lower PET, reaching values of less than 1600 mm/yr.

In the upper Fincha'a basin, there are two very large swamps. The Chomen Swamp is the larger of the two, with a drainage area of about 860 km^2, of which about 265 km^2 are occupied by the swamps immediately downstream of the Chomen Swamp.

2.1.6 Soil type

The soil data is a significant component in the study of how LULCC can impact the hydrological components of a watershed. According to a previous study performed by Makin [17], the soil type in the study area is closely related to parent materials, degree of weathering and the characteristics of the local reliefs. The main parent materials are basalt, ignimbrite, acid lava, volcanic ash and pumice.

The soil map of the study area was obtained from the Ministry of Water, Irrigation and Electricity of Ethiopia. According to the FAO/UNESCO classification [18], six major soil groups were identified in the Fincha'a watershed: Eutric Nitosols, Eutric Cambisols, Water, Chromic Vertisols, Cambic Arenosols and Dystric Cambisols (Table 2). Besides the location of each soil type, the Ministry of Water, Irrigation and Electricity of Ethiopia provided also information about soil physical and chemical properties such as soil texture, available water content, bulk density, hydraulic conductivity and organic carbon content.

The SWAT model has predefined four-letter codes for each land use category. These codes were therefore used to link or associate the land use map of the study area to the SWAT land-use databases.

Table 2. Soils that are present in the Fincha'a watershed.

Soil Name	Area covered		SWAT naming
	[ha]	[%]	
Dystric Cambisols	437.1643	0.14	Bd31-2c-11
Eutric Cambisols	94827.3963	29.57	Be8-3c-24
Cambic Arenosols	35365.7764	11.03	Qc5-1c-182

Preprints (www.preprints.org) | NOT PEER-REVIEWED | Posted: 28 July 2021 doi:10.20944/preprints202107.0630.v1

Eutric Nitosols	113078.3254	35.27	Ne20-3b-160
Chromic Vertisols	35579.3598	11.10	Vc23-3a-262
Water	41360.6536	12.90	WR-192

Figure 9 shows the soil map of the Fincha'a watershed, pointing out the major presence of Cambric Arenosols in the northern part of the basin, while the southern area is largely covered by water.

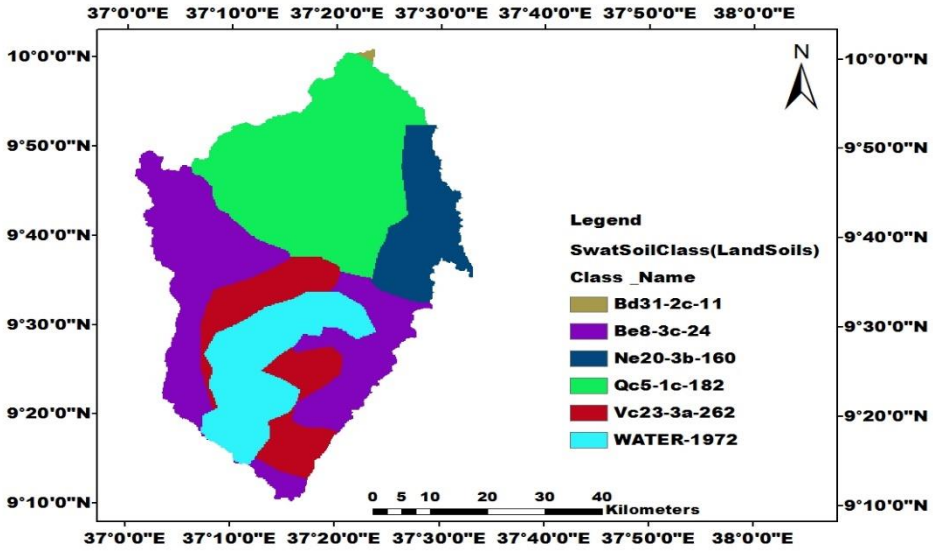

Figure 9. Soil map of the Fincha'a watershed. The legend shows the SWAT naming of the soils.

2.2 Spatial Data and Satellite imagery

Besides information on the local hydrology and soil composition, the present study requires also a Digital Elevation Model (DEM) and satellite images for deriving LULC. This information was derived from multiple sources, such as the Ministry of Water, Irrigation and Energy Resource Office, National Meteorological Agency, and Nile Basin Authority offices.

2.2.1 Digital Elevation Model

For this study, the Digital Elevation Model of the whole Ethiopia (spatial resolution 30m by 30m) was obtained from the Nile Basin Authority Office, and then the Fincha'a watershed DEM was clipped using Arc-GIS to obtain the input data for the SWAT model (Figure 10). It was projected to Addenda and UTM Zone 37 to create an overlay with soil and land use raster dataset using Arc-GIS 10.5.1.

The same Arc-GIS software was also used to process the DEM and create a triangulated irregular network for deriving both the river network and the flood inundation maps.

Preprints (www.preprints.org) | NOT PEER-REVIEWED | Posted: 28 July 2021 doi:10.20944/preprints202107.0630.v1

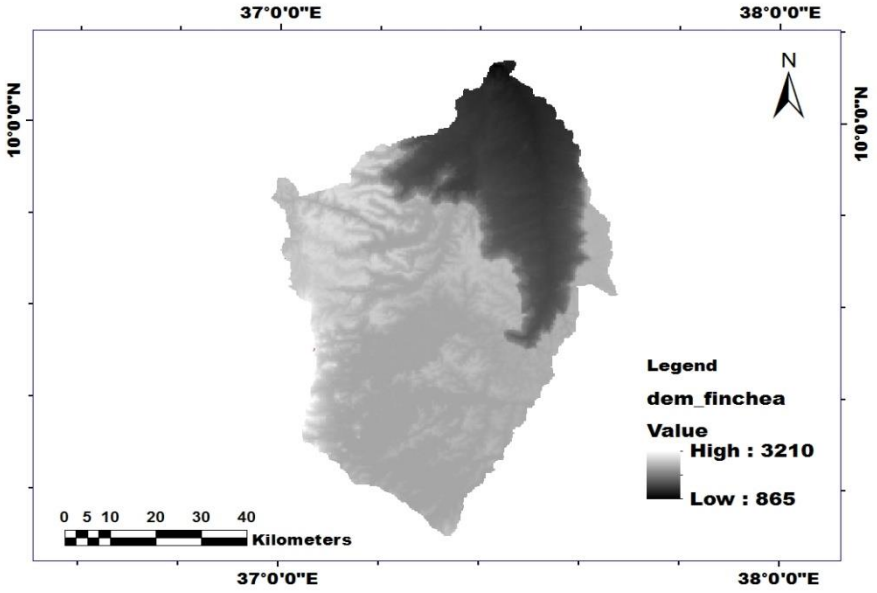

Figure 10. Digital Elevation Model of the study area.

2.2.3 Landsat imagery

Landsat satellite images were analysed to identify changes in land use land cover distribution in the Fincha'a watershed over 25 years (from 1994 to 2018). For this period, three Landsat images of 1994, 2004 and 2018 were downloaded from the United States Geological Survey website (earthexplorer.usgs.gov) GeoTIFF file format. Landsat TM, ETM, and OLI/TIRS were selected to represent the land cover conditions in the years 1994, 2004 and 2018, respectively. Landsat sensors have a variable spatial resolution, depending on the bands: 15, 30 or 60 m [19]. Landsat images were geo-referenced to WGS_84 datum and Universal Traverse Mercator (UTM) Zone 37N. Preprocessing such as layer stacking, mosaicking and band colour combination were carried out to orthorectify the images, using ERDAS Imagine 2014 and GIMP 2.10.12 software.

The false-colour composites of the satellite images of the Fincha'a watershed during 1994, 2004, and 2018 are given in Figures 11, 12 and 13, respectively.

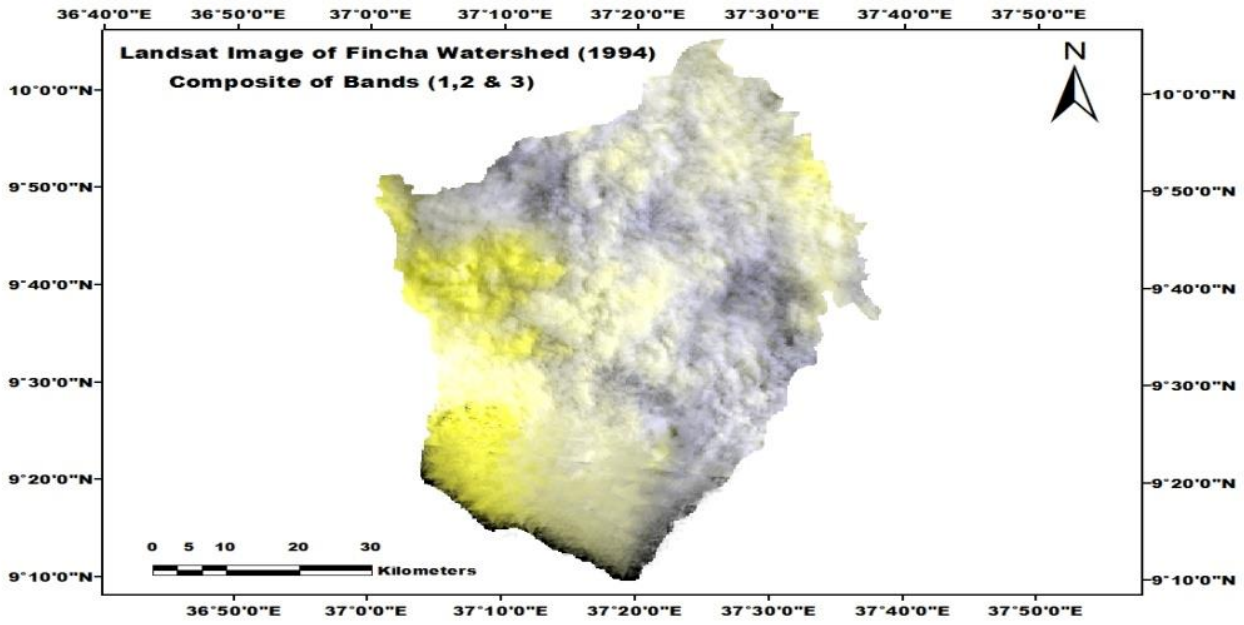

Preprints (www.preprints.org) | NOT PEER-REVIEWED | Posted: 28 July 2021 doi:10.20944/preprints202107.0630.v1

Figure 11. False-colour composite of satellite images of the Fincha'a watershed acquired in 1994.

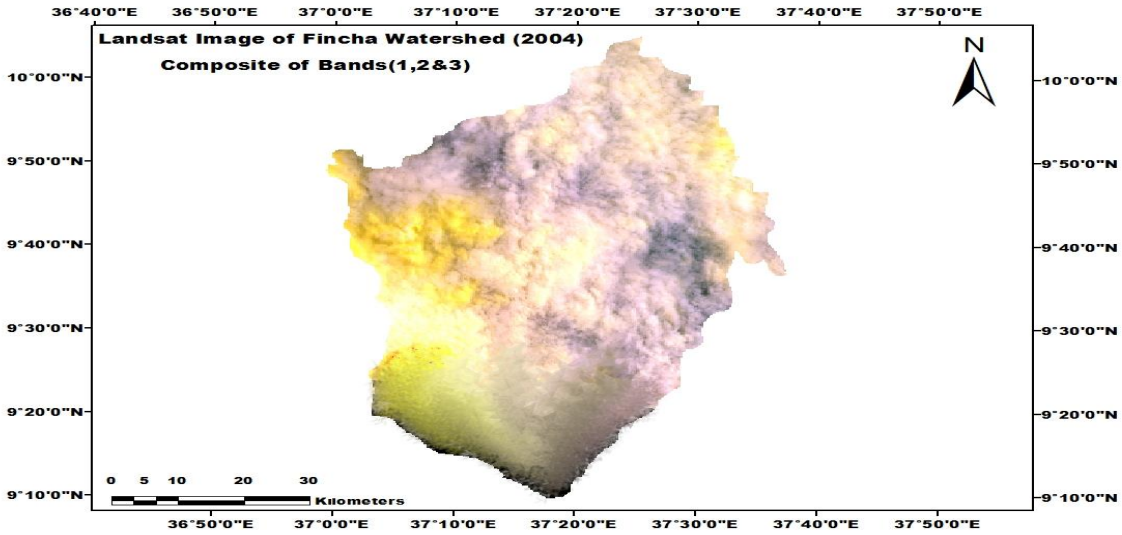

Figure 12. False-colour composite of satellite images of the Fincha'a watershed acquired in 2004.

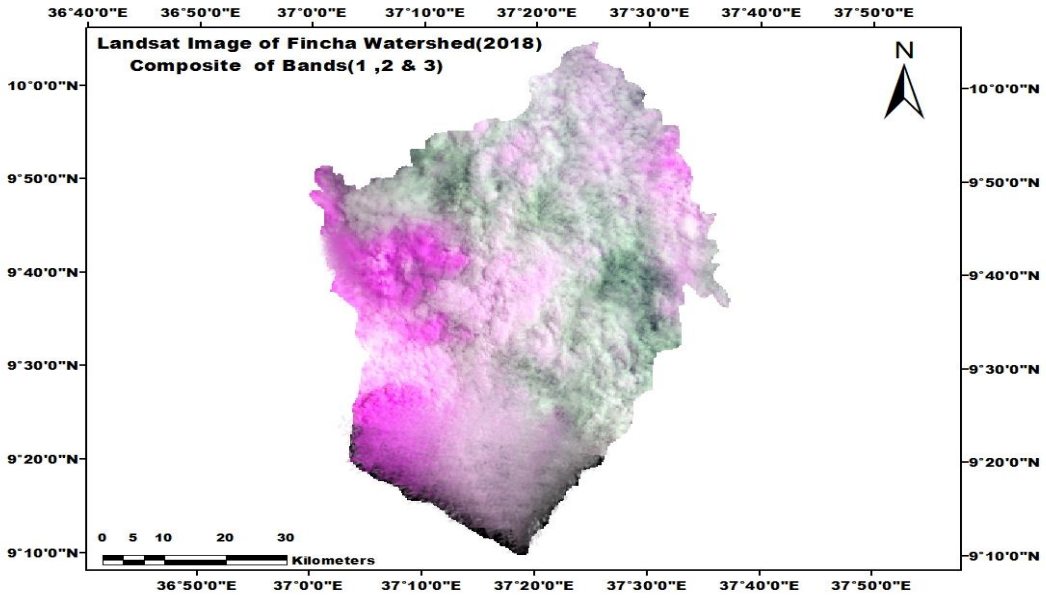

Figure 13. False-colour composite of satellite images of the Fincha'a watershed acquired in 2018.

Table 3 reports the details of the used Landsat image.

Table 3. Attributes of Landsat images.

Sensor	Spatial resolution	Acquisition date	Image quality	Path/Row
Landsat 5 TM	30 m	5/01/1994	7	169/053
Landsat 7 ETM	30 m	07/12/2004	9	169/053
Landsat 8 OLI/TRIS	30 m	03/12/2018	9	169/053

source: www.usgs.gov

Preprints (www.preprints.org) | NOT PEER-REVIEWED | Posted: 28 July 2021 doi:10.20944/preprints202107.0630.v1

2.3 Image Classification Process

Image classification is the process of sorting pixels into a finite number of individual classes or categories of data based on their data file values. In remote sensing, there are various image classification methods, supervised, unsupervised and hybrid. Unsupervised classification is computer controlled and its limitation is that the user cannot control the computer's selection of pixels into clusters. In the case of a supervised image classification system, the user relies on her/his prior knowledge and skills and can select a group of pixels belonging to a particular LULC. In this system, the user is required to have good knowledge about the local conditions of the area under study, or clear field evidence to validate the classification. Supervised classification is the most common type of land use classification system and depends on prior information about the land use and land cover.

2.3.1 Supervised Classification

The present analysis was performed employing the supervised classification method, using previous studies of Bezuayehu [20] and Taye [21] as a reference for classification numbers. Using the Landsat 7 images acquired in 2004, eight classes of LULC such as cultivated land, bare soil, forest land, shrubland, grassland, settlement, waterbody and wetland were produced (Table 4):

- Cultivated Land: areas used for crop cultivation, both annuals and perennials, and the scattered rural settlements that are closely associated with the cultivated fields.
- Bare Soil: areas covered with soil surfaces and sand with no vegetation cover or uncultivated farmlands consisting of exposed soil and rock outcrops.
- Forest Land: land covered with dense trees which include evergreen forest land, mixed forest and sparse trees.
- Shrub Land: land covered with open shrubs, closed shrubs, bushes, and mixed with small trees.
- Grass Land: areas covered with grass used for grazing, as well as bare lands that have little grass or no grass cover. It also includes other small-sized plant species.
- Settlement: area covered with building rural residential houses infrastructures roads.
- Waterbody: waterlogged areas and lakes throughout the year, the rivers and their main tributaries.
- Wetlands: an area that is saturated with water, either permanently or seasonally waterlogged around swamp area.

Table 4. Land use classification of the Fincha'a watershed, and corresponding SWAT code.

S.no	Land use/land cover	SWAT LULC	SWAT code
1	Cultivated Land	Agricultural land row crops	AGRR
2	Bare Soil	Barren	BARR
3	Forest Land	Forest-Evergreen	FRSE
4	Shrub Land	Forest-Mixed	FRST
5	Grass Land	Agricultural Land-Generic	AGRL
6	Settlement	Residential	URBN
7	Waterbody	Water	WATR
8	Wetland	Wetlands-Mixed	WETL

Since there may be misclassification of pixels in supervised classification, it is necessary to test the accuracy of the classification by using ground truth, as well as assessing the accuracy via confusions matrixes, as described in Section 3.2.

In fact, a paramount step in the classification process, whether supervised or unsupervised, is the accuracy assessment of the final classification produced. This involves

Preprints (www.preprints.org) | NOT PEER-REVIEWED | Posted: 28 July 2021 doi:10.20944/preprints202107.0630.v1

identifying a set of sample locations that have field evidence, or using previous studies. The land use and land cover found in the field is then compared to the one mapped in the image for the same location. Then, statistical assessment of accuracy may then be derived for the entire study area. Generally, accuracy assessment is a very important measurement to determine how accurate the referenced data agree with classified images of the remotely sensed data [22].

The error matrix produced may be used to identify specific cover types for which errors are in excess of that desired. The information in the matrix about which covers are being mistakenly included in a particular class (error of commission) and those that are being mistakenly excluded (errors of omission) from that class can be used to refine the classification approach.

2.4 Hydrological Modeling with SWAT

2.4.1 Model Setup

Arc-SWAT version 2012.10_4.19 was downloaded from the SWAT website (swat.tamu.edu) and its toolbar was added to Arc-GIS 10.5.1 for the modelling process. The modelling procedure includes SWAT project setup, watershed delineation, Hydrologic Response Units (HRU) analysis, write input tables, edit SWAT input and SWAT simulation. After data collection, all the input data were prepared, the watershed was delineated, the HRUs definition were defined, and the land-use/soil/slope classification was added to the model. The model was run at the basis scale, assuming three years of the warm-up period. The details of each step are provided in the following.

2.4.2 Watershed Delineation

The first step in generating a SWAT model is the watershed delineation. The soil map, the LULC map and the DEM were projected using Arc-GIS 10.5.1 to the same projection system before watershed delineation, to assure maps overlapping. The watershed and sub-watershed delineations were performed using the 30mx30m DEM. The obtained slope classes are shown in Table 5 and Figure 14.

Table 5. Slope classes.

Slope	**% area**	**Area** [ha]
0-3	22.43	71925.8021
3-8	29.93	95965.2960
8-15	21.07	67548.7056
15-30	18.08	57980.1691
>30	8.49	27228.7031

Preprints (www.preprints.org) | NOT PEER-REVIEWED | Posted: 28 July 2021 doi:10.20944/preprints202107.0630.v1

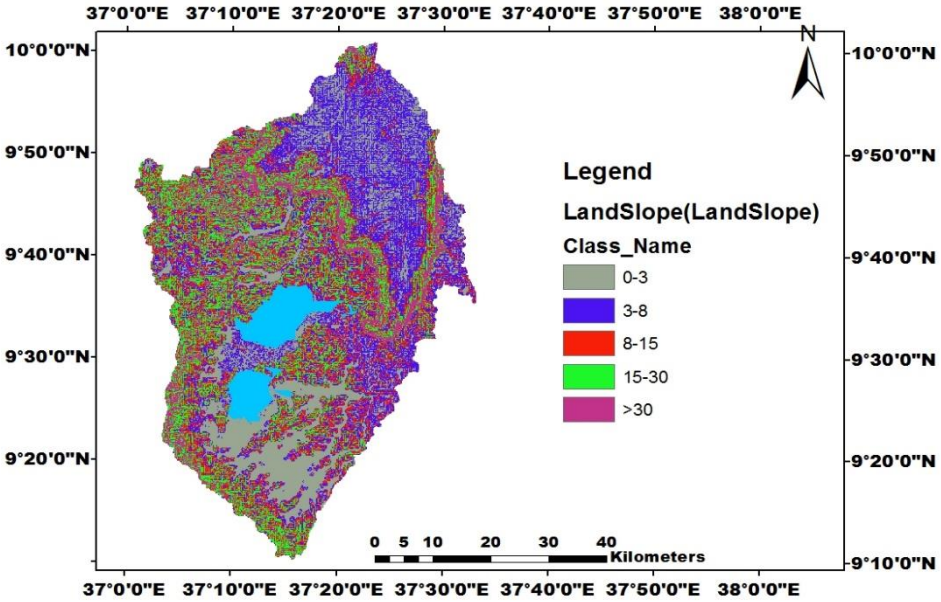

Figure 14. Slope classes in the Fincha'a watershed.

2.4.3. Hydrologic Response Units

After the watershed delineation, land use, soil and slope characterization were performed using commands from the HRU analysis menu on the Arc-SWAT toolbar. These tools were used in loading land use and soil layers of the Fincha'a watershed into the current project, to evaluate the slope characteristics and determine the land use/soil/slope class combinations and distributions for each sub-basin.

The SWAT user's manual suggests that a 20% land use threshold, 10% soil threshold and 20% slope threshold are adequate for the most common modelling applications. However, Setegn et al. [23] suggested that the HRU definition with multiple options that account for 10% land use, 20% soil and 10% slope threshold combinations gives a better estimation of runoff and sediment components in Ethiopian regions. Therefore, for this study, the HRU definition was performed using such thresholds. The Fincha'a watershed was divided into 176 HRUs and 18 sub-basins, having their unique land use and soil combinations (Table 6).

Table 6. Hydrologic Response Units and dominant LULC

Sub-basin	Number of HRUs	Dominant LULC	% area
1	19	FRSE	63.32
2	7	uniform FRSE	3.25
3	8	uniform FRSE	1.69
4	15	FRSE	3.33
5	16	AGRR	1.38
6	8	uniform FRSE	3.19
7	5	FRSE	1.43
8	10	AGRR	4.95
9	11	WATR	0.71
10	5	AGRR	0.37
11	9	FRSE	2.08
12	6	AGRR	0.84
13	14	AGRR	1.96
14	8	AGRR	4.08
15	6	WATR	0.02

Preprints (www.preprints.org) | NOT PEER-REVIEWED | Posted: 28 July 2021 doi:10.20944/preprints202107.0630.v1

16	14	AGRR	3.4
17	6	AGRR	0.09
18	9	AGRR	3.85
Total	176		100

2.4.4 Weather Data

The weather data can be imported into the SWAT model considering six categories: weather generator data, rainfall data, temperature data, solar radiation data, wind speed data and relative humidity data. The weather generator can be used in the case of missing values in the dataset collected from the meteorological stations [24].

The SWAT model requires daily hydro-meteorological data from measured data or generated from values using monthly average data. Thanks to the data availability, in this study data measured at the daily scale were used, eventually applying the SWAT weather generator in the case of missing values.

Weather data of the Homi station was used as an input to determine the value of the weather generator parameters. These parameters (rainfall, temperature, relative humidity, solar radiation, wind speed) were developed by using a pivot table, dew point temperature calculator software, DEW02 and PCP stat to calculate average monthly and average daily precipitation, standard deviation, skew coefficient, probability of a wet day following a dry day and the average number of days of precipitation in a month.

2.4.5 Sensitivity Analysis

Sensitivity analysis is defined as the process of determining the significance of one or a combination of parameters with respect to the objective function or a model output [25]. Before the SWAT calibration and validation process, a sensitivity analysis was carried out to reduce the number of parameters that needs optimization.

In this research, a semi-automated Sequential Uncertainty Fitting (SUFI 2) was applied to identify the sensitive parameters, by selecting the most flow influencing parameters in the catchment. The t-Stat and P-Values of the parameters were used to rank the different parameters that may influence the flow and finally to select the ranked values. The model was run on a monthly basis with observed data of the Fincha'a River at the outlet of the Fincha'a dam site. Based on previous studies, 26 parameters were selected for investigating their effects on the final results, but only 12 parameters were finally identified to have a significant influence in controlling the streamflow in the watershed.

2.4.6 Calibration and Validation

After sensitivity analysis, the identified parameters were used for model calibration, considering the period 1997-2004. A preliminary manual calibration was done and some parameters were adjusted in the SWAT model. After this, the model was run using the best parameter output values and the simulations were compared with observed streamflow data using Nash-Sutcliffe coefficient (*NS*), coefficient of determination (R^2) and percent bias (*PBIAS*).

The validation was performed to compare the model outputs with an independent dataset without making a further change to parameters obtained during the calibration process. The measured data of average monthly streamflow from 1997-2008 at the outlet section of Chomen Lake was used for validating the SWAT model.

2.4.7. Model Performance Evaluation

The evaluation of the model performance was done following the approach proposed by Da Silva [26]: Nash Sutcliffe coefficient (*NS*), coefficient of determination (R^2) and percent bias (*PBIAS*) were used to quantify the accuracy in watershed modelling.

The coefficient of determination (R^2) describes the proportion of variance in measured data by the model (eq. 2). It indicates the linear relationship between simulated and

Preprints (www.preprints.org) | NOT PEER-REVIEWED | Posted: 28 July 2021 doi:10.20944/preprints202107.0630.v1

observed data and ranges from 0-1 (the relation between measured data and simulated data is poor when R^2 is 0 and there is a good relationship between the two when the value approaches 1).

$$R2 = \frac{\sum_i (Q_m - \overline{Q_m})(Q_s - \overline{Q_s})^2}{\sum_i (Q_m - \overline{Q_m})^2 (Q_s - \overline{Q_s})^2} \quad (2)$$

where R^2 is the coefficient of determination, Q_m and Q_s are the measured and simulated values, respectively, while $\overline{Q_m}$ and $\overline{Q_s}$ *are their* averages.

The Nash-Sutcliffe simulation efficiency (*NS*) describes the deviation from the unit of the ratio of the square of the difference computed between the observed and simulated values and the variance of the observations (eq. 3). Following a simplified explanation provided by Moriasi et al. [12], the Nash-Sutcliffe parameter represents an indication of how well the plot of observed versus simulated data fits the 1:1 line.

$$NSE = 1 - \left[\frac{\sum_i (Q_m - Q_s)^2}{\sum_i (Q_m - \overline{Q_m})^2}\right] \quad (3)$$

The percent bias (*PBIS*) describes the tendency of the simulated data to be greater or smaller than the observed data, expressed as a percentage (eq. 4):

$$PBIAS = 100 \left[\sum_i \frac{Q_m - Q_s}{\sum_i Q_m}\right] \quad (4)$$

3. Results and Discussion

3.1 Land Use Land Cover Change

Land use/land cover of the Fincha'a Watershed were observed for three reference years (1994, 2004 and 2018) using Landsat satellite imagery and supervised classification, and compared accounting for eight classes (Table 4). For qualitative comparison, Figures 15 and 16 were created, while the quantitative information is reported in Table 7, pointing out a very relevant change in LULC over the study period.

A rapid increase in the cultivated land class is observable during the study period, as this class occupied 42.84% of the total area in 1994 but 70.06% in 2018. As pointed out in similar studies [5], this is due to population growth and socio-economic factors. The bare soil and settlement also gradually increased from 1.68% (1994) to 4.25% (2018) and 0.08% (1994) to 0.35% (2018), respectively. The increment of bare soil can be explained as the result of erosion and the steep slopes of the Fincha'a watershed, while the need for more room for a growing population is obviously the cause of a major percentage of settlements. The water body and wetland features such as rivers, lakes and swamps were slightly increased from 10.32% (1994) to 18.57 % (2018) and 0.69% (1994) to 4.36% (2018), respectively.

On the contrary, other land use classes decreased over the 25 years study period. For instance, forest land has been greatly decreased from 33.46% in 1994 to only 1.16% in 2018, with a net decline of 32.1, mostly because of the expansion of agricultural land. Urbanization and agricultural expansion cause also a reduction of the areas covered by shrub and grass, which were degraded by a net percent of 9.56% and 0.12%, respectively.

Table 7. LULC in the Fincha'a watershed in 1994, 2004 and 2018. LULCC between 1994 and 2018.

LULC	1994		2004		2018		2018-1994	
	%	**Area** [ha]	%	**Area** [ha]	%	**Area** [ha]	%	**Area** [ha]
Cultivated Land	42.84	137352.31	59.25	189976.87	70.06	224624.24	+87271.94	+27.22
Bare Soil	1.68	5376.85	3.52	11265.78	4.25	13600.26	+8223.42	+2.57

Preprints (www.preprints.org) | NOT PEER-REVIEWED | Posted: 28 July 2021 doi:10.20944/preprints202107.0630.v1

Forest Land	33.46	107283.40	13.01	41714.20	1.16	3719.33	-103564.07	-32.3
Shrub Land	10.78	34565.07	7.15	22925.81	1.22	3910.08	-30654.99	-9.56
Grass Land	0.15	488.97	0.12	391.18	0.03	97.79	-391.18	-0.12
Settlement	0.08	262.66	0.16	525.32	0.35	1161.86	+899.20	+0.27
Water Body	10.32	33101.79	14.25	45707.42	18.57	59563.98	+26462.19	+8.25
Wetland	0.69	2217.63	2.54	8163.46	4.36	14012.86	+11795.23	+3.67
Total	100	320648.68	100	320045.70	100	348016.75		

In 1994, cultivated land and forest land were 42.84% (137352.31 ha) and 33.46% (107283 ha), respectively, while shrubland, waterbody, bare soil, wetland, grassland and settlement area were 10.78% (34565.07 ha), 10.32% (33101.79 ha), 1.68% (5376.85 ha), 0.69% (2217.63 ha), 0.15% (488.97 ha) and 0.08% (262.66), respectively. Therefore, in this specific year, cultivated land and forest land were the dominant classes.

In 2004, cultivated land and forest land were 59.25% (189976.87ha) and 13.01% (41714.20 ha), while shrubland, waterbody, bare soil, wetland, grassland and settlement were 7.15% (22925.81ha), 14.25%(45707.42ha), 3.52% (11265.78ha), 2.54% (8163.46 ha), 0.12% (391.18ha) and 0.16% (525.32ha), respectively. Further, throughout the study period, cultivated land has been the most dominant land use class.

In 2018, cultivated land and forest land were respectively 70.06% (224624.24 ha) and 1.16% (3719.33 ha), while shrubland, waterbody, bare soil, wetland, grassland and settlement were 1.22% (3910.08 ha), 18.57% (59563.98 ha), 4.25% (13600.26 ha), 4.36% (14012.86 ha), 0.03 (97.79 ha) and 0.35% (1161.86 ha), respectively. The result shows that, in 2018, grassland and forest land were negligible and cultivated land is the most predominant LULC class in the Fincha'a watershed.

Preprints (www.preprints.org) | NOT PEER-REVIEWED | Posted: 28 July 2021 doi:10.20944/preprints202107.0630.v1

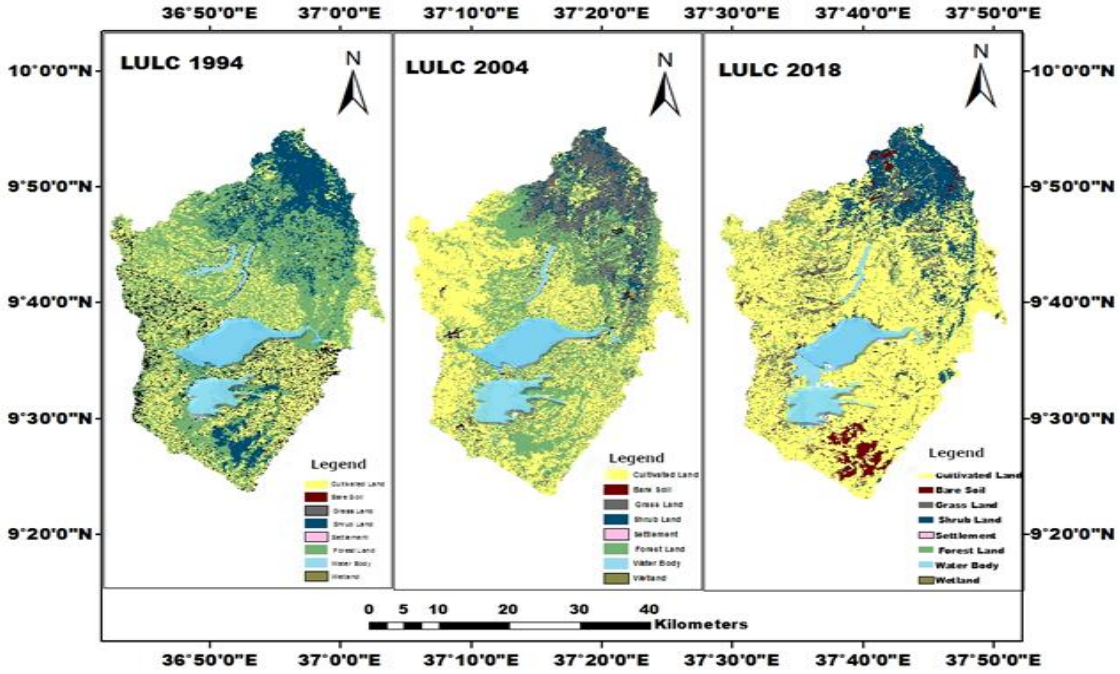

Figure 15. Fincha'a watershed LULC in the three reference years.

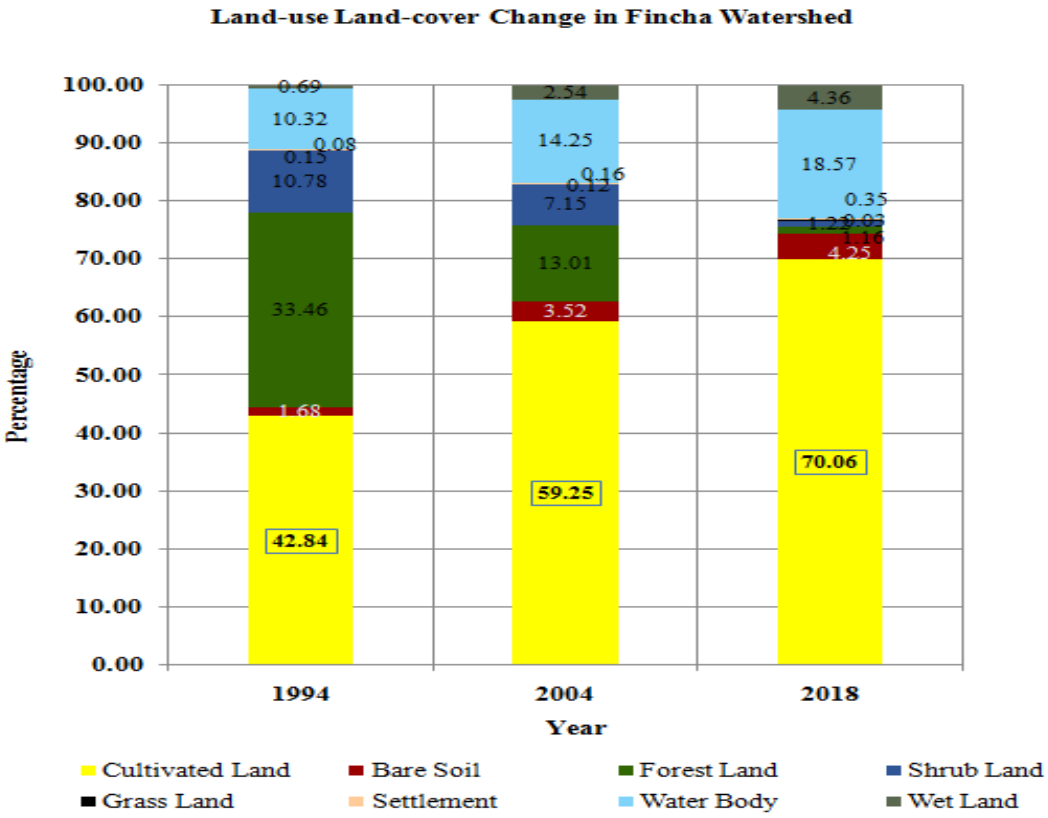

Figure 16. Percentage of LULC distribution in Fincha'a Watershed in the three reference years.

3.2 Land Use Classification Accuracy

Preprints (www.preprints.org) | NOT PEER-REVIEWED | Posted: 28 July 2021 doi:10.20944/preprints202107.0630.v1

In this study, the random reference points are 178, 249 and 318 for the years 1994, 2004 and 2018, respectively. To assess the classification accuracy, confusion matrixes were derived using ERDAS Imagine 2014 and GIMP 2.10.12 software.

Tables 8, 9 and 10 show the confusion matrix for the three Landsat images, pointing out that the overall classification accuracy of the total number of correctly classified pixels (diagonal) to the total number of reference pixels was 92.52%, 92.71% and 94.44% for 1994, 2004 and 2018, respectively. According to Anderson [8], the minimum accuracy value for reliable land cover classification is 85%, therefore the results presented here satisfy the minimum accuracy assessment criteria. The user's accuracy (error of commission or inclusion) and producers' (error of omission or exclusion) which are used to evaluate classification accuracy were also calculated.

Table 8 shows that, for the reference year 1994, the percentage of overall accuracy and kappa coefficient were 86.06% and 83.61%, respectively. The grey-highlighted diagonal number in the matrix indicated correctly classified pixels for each LULC class, with the yellow cell indicating the total number of correctly classified pixels.

Table 8. Confusion matrix of LULC in 1994 (S: Settlement, WL: water body, SHL: Shrub Land, CL: cultivated land, GL: grassland, FL: forest land, BS: bare soil).

LULC	S	WL	SHL	WB	CL	GL	FL	BS	Total	User (%)
S	8	0	1	0	1	0	2	0	12	66.67
WL	1	18	0	2	0	1	0	1	23	78.26
SHL	0	1	15	0	2	0	0	0	19	78.95
WB	1	0	1	21	0	0	1	0	24	87.50
CL	0	3	0	0	27	1	0	0	31	87.10
GL	0	0	0	0	0	15	3	2	20	75.00
FL	0	2	0	0	0	0	33	1	36	91.67
BS	0	0	0	0	0	2	0	16	20	100.00
Total	10	24	16	23	30	19	36	20	178	OA=86.06
Producer's (%)	80.00	75.00	93.75	91.30	90.00	78.95	91.67	80		Ka=83.61

Over all Classification Accuracy (OA) =86.06%, Kappa coefficient (K) =83.61%

Table 9 shows that the classified map of 2004 has an overall accuracy of 89.16% and a kappa coefficient of 87.43%. In this case, it is possible to notice a higher number of pixels correctly classified.

Table 9. Confusion matrix of LULC in 2004 (S: Settlement, WL: water body, SHL: Shrub Land, CL: cultivated land, GL: grassland, FL: forest land, BS: bare soil).

LULC	S	WL	SHL	WB	CL	GL	FL	BS	Total	User's (%)
S	10	1	0	1	0	0	1	0	13	76.92
WL	0	35	1	0	2	0	0	0	38	92.11
SHL	1	0	32	0	0	0	0	1	34	94.12
WB	0	0	1	33	0	2	0	0	36	91.67
CL	0	0	0	0	40	0	2	1	43	93.02

Preprints (www.preprints.org) | NOT PEER-REVIEWED | Posted: 28 July 2021 doi:10.20944/preprints202107.0630.v1

GL	0	0	3	0	3	20	0	0	26	76.92
FL	0	1	0	1	0	2	34	0	38	89.47
BS	0	0	0	0	0	3	0	18	21	85.71
Total	11	37	37	35	45	27	37	20	249	OA=89.16
Producer's (%)	90.91	94.59	86.49	94.29	88.89	74.07	91.89	90.00		Ka=87.43

Over all Classification Accuracy (OA) =89.16%, Kappa coefficient (K) =87.43%

In 2018, the overall accuracy and kappa coefficients were 92.45% and 91.30%, respectively (Table 10), with the highest number of correctly classified pixels during the study period.

Table 10. Confusion matrix of LULC in 2018 (S: Settlement, WL: water body, SHL: Shrub Land, CL: cultivated land, GL: grassland, FL: forest land, BS: bare soil).

LULC	S	WL	SHL	WB	CL	GL	FL	BS	Total	User's (%)
S	15	0	0	0	1	2	0	0	18	83.33
WL	0	43	1	0	0	0	1	0	45	95.56
SHL	1	0	40	1	0	1	0	1	44	90.91
WB	0	1	0	41	1	0	0	0	43	95.35
CL	0	0	1	0	48	0	2	1	52	92.31
GL	0	1	0	2	0	30	0	0	33	90.91
FL	1	0	0	0	1	1	42	0	45	93.33
BS	0	1	1	0	0	0	1	35	38	92.11
Total	17	46	43	44	51	34	46	37	318	OA=92.45
Producer's (%)	88.24	93.48	93.02	93.18	94.12	88.24	91.30	94.59		Ka=91.30

Over all Classification Accuracy (OA) =92.45%, Kappa coefficient (K) =91.30%

3.3 Calibration and validation of the streamflow

The simulated streamflow was calibrated against observed discharge, considering a period of 8 years (1997-2004) and monthly data. The first three years were used as the warm-up period, while the rest were for model calibration. The coefficient of determination and the Nash- Sutcliffe equation (Section 2.4.7) has been used as parameters to determine the quality of the performed calibrations. As visible from Figure 17, the SWAT model is able to reproduce the measured water flow in a rather satisfactory manner (R^2=0.86, *NSE*=0.85), with a slight underestimation of the peaks.

Preprints (www.preprints.org) | NOT PEER-REVIEWED | Posted: 28 July 2021 doi:10.20944/preprints202107.0630.v1

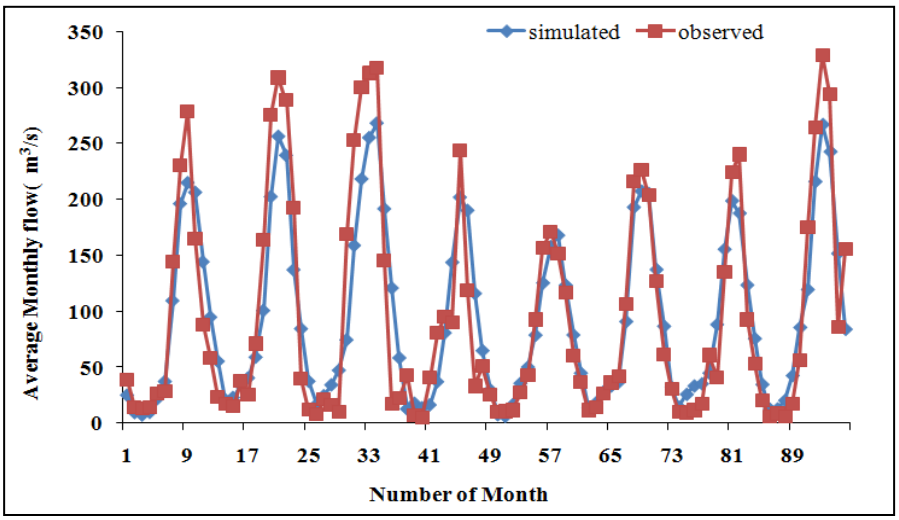

Figure 17. Simulated and observed flow during the calibration period (1997-2004).

The Fincha'a streamflow was validated for four years, between 2005 and 2008. As visible in Figure 18, the validation processes provided good results, with a correlation coefficient R^2=0.87 and a Nash-Sutcliffe coefficient *NSE*=0.84. Also in this case it is possible to observe an underestimation of the peak conditions which, however, does not influence the overall simulation.

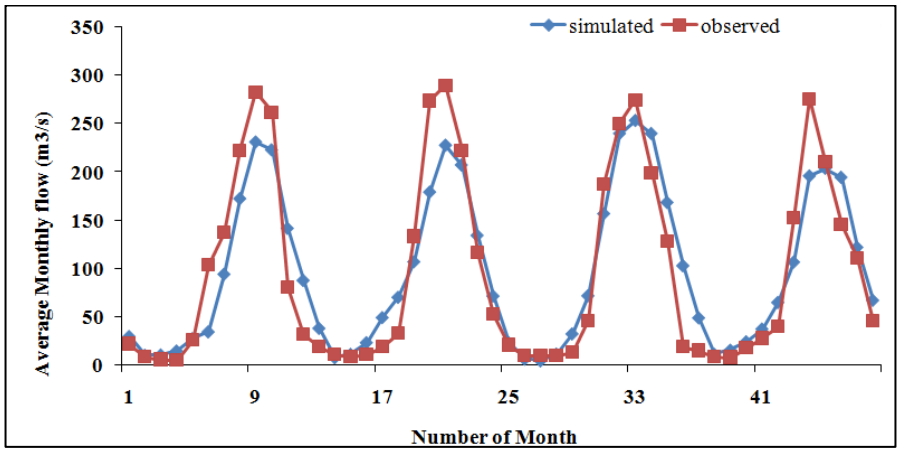

Figure 18. Simulated and observed flow during the validation period (2005-2008).

Table 11 summarizes the parameters used for evaluating the model performance during the calibration and validation process (see Section 2.4.7), while Figure 19 provides a scatter plot of the simulated and observed flow values for the two periods. Based on such results, it can be concluded that the SWAT model can be applied to have a reliable prediction of the streamflow of the Fincha'a watershed.

Table 11. Model performance evaluation statics.

	R^2	NSE	PBIAS
Calibration (1997-2004)	0.86	0.85	+1.13
Validation (2005-2008)	0.87	0.84	-2.806

Preprints (www.preprints.org) | NOT PEER-REVIEWED | Posted: 28 July 2021 doi:10.20944/preprints202107.0630.v1

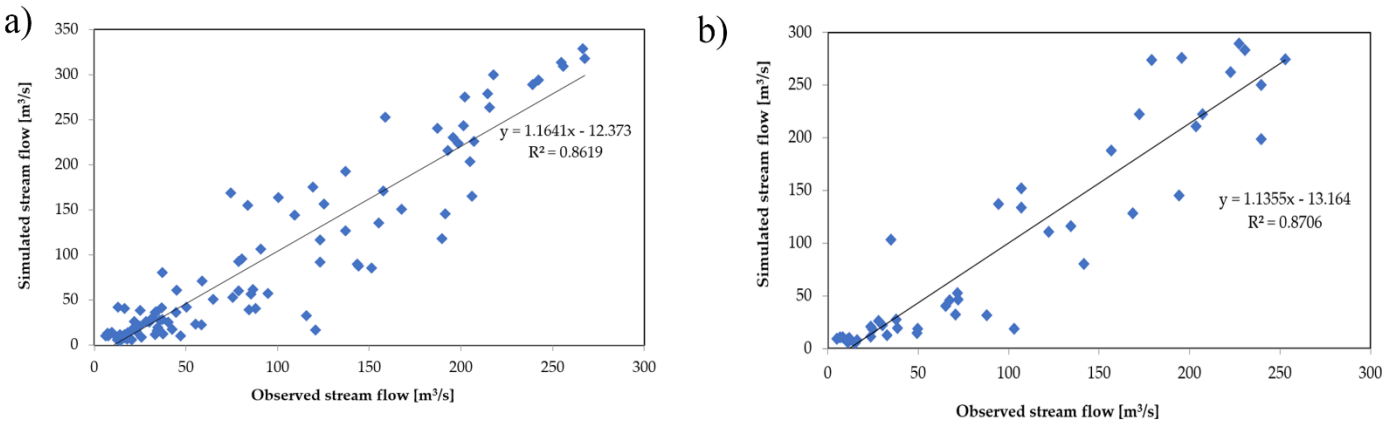

Figure 19. Scatter plot of simulated and observed flow during the **a)** calibration (1997-2004) and **b)** validation (2005-2008) periods.

3.4 Hydrological Response to LULC changes on streamflow.

As already observed, the hydrologic responses of watershed processes are generally highly affected by LULCC [27]. Crucial watershed processes that can be affected by LULCC are surface runoff, lateral flow and groundwater flow

Table 12 shows the stream flow simulated accounting for the LULC situation in the three reference years, classifying it into wet (August, September and October) and dry months (February, March and April).

Table 12. Observed average flow during the dry and wet months.

period	**Average flow** [m³/s]			**Change of flow** [m³/s]		
	1994	**2004**	**2018**	**1994-2004**	**2004-2018**	**1994-2018**
dry months	10.72	15.89	25.86	+5.17	+9.47	+14.64
wet months	132.67	167.85	194.67	+35.18	+26.82	+62.00

It is possible to notice that the average dry monthly streamflow increased by 5.17 m³/s between 1994 and 2004, 9.47m³/s from 2004 to 2018 and 14.64 m³/s over the whole period (1994 - 2018). This means that, during the 25 years, the dry-months discharge increased by 8.25%. The average wet month flow was more influenced by LULCC, increasing by 35.18 m³/s, 26.82 m³/s and 62 m³/s between 1994-2004, 2004-2018 and 1994-2018, respectively.

This analysis can reveal that the increment of cultivated land causes a direct increase in surface runoff, in particular during the wettest months. Changes in the areas covered by wetland and water bodies cause also a slight increase in flow discharge during the driest months.

3.5 Sensitivity analysis

As anticipated in Section 2.4.5, the sensitivity analysis pointed out that, out of 26 possible parameters, only twelve have a relevant influence in controlling the hydrological processes in the watershed (Table 12). Based on a previous work of Leta et al. [13], saturated hydraulic conductivity, base flow alpha factor, groundwater delay and the depth of the water aquifer were considered the most important sensitive parameters to be used in the calibration process.

Table 13. Streamflow sensitivity parameters.

Preprints (www.preprints.org) | NOT PEER-REVIEWED | Posted: 28 July 2021 doi:10.20944/preprints202107.0630.v1

S.no	Parameter	Definition	Fitted value	Max_value	Min_value
1	SOL_K	Saturated Hydraulic conductivity	0.24	-0.8	0.8
2	ALPHA_BF	Base flow alpha factor (days)	0.85	0	1
3	GW_DELAY	Ground water delay (days)	51	30	450
4	GWQMN	The threshold depth of water shallow aquifer	0.3	0	2
5	GW_REVAP	Groundwater revamp coefficient	0.11	0	0.2
6	ESCO	Soil evaporation compensation factor	0.93	0.8	1
7	CH_N2	Manning's roughness coefficient	0.045	0	0.3
	CH_K2				
8		Effective hydraulic conductivity	23.75	5	130
9	ALPHA_BNK	Baseflow alpha factor for bank storage	0.45	0	1
10	SOL_AWC	Soil available water capacity	-0.17	-0.2	0.4
11	CN2	SCS runoff Curve number for moisture condition II	-0.18	-0.2	0.2
12	SOL_BD	Moist bulk density	0.105	-0.5	0.6

4. Conclusions and Recommendations

4.1 Conclusions

This study has shown that the SWAT model can be successfully applied to examine the hydrological responses to LULCC in the Ethiopia Fincha'a watershed. To do this, satellite images were used to produce LULC maps for three reference years, chosen within 25 years (1994-2018). Once determined the most significant classes covering the whole basin, weather and hydrological data, combined with a topographical base derived from a rather coarse DEM, can be used to infer information on the surface runoff over the entire watershed.

Comparing the LULC derived from satellite images, it is possible to observe a significant decline of forest land (-32.3%) and shrubland (-9.56%) between 1994 and 2018, mostly because of the creation of new agricultural zones (+27.22%) and settlement (+3.67%) to answer to an increasing population that needs new means of subsistence. The quality of the supervised classification used for deriving LULC maps was checked via confusion matrixes, showing an overall accuracy, for 1994, 2004 and 2018 respectively, of 86.06%, 89.16% and 92.45% and corresponding kappa coefficients of 83.61%, 87.43% and 91.30%.

The overall efficiency of the SWAT model was evaluated by both the coefficient of determination and the Nash-Sutcliffe parameters, which resulted always higher than 0.84 for both the calibration and validation periods, indicating that the model here proposed provided reliable outcomes. Once calibrated and validated, the model was applied and the outcomes pointed out that the LULCC observed in the Fincha'a basin caused an increase in surface runoff, more prominent during the wet months (August-October).

As similar research performed across Ethiopia have pointed out [see review 5], this study provides important insights on the basin-wide effects of LULCC on the Fincha'a catchment hydrology, to be used by decision-makers for planning future management strategies to assure a suitable future of the country.

4.2 Recommendations

Based on the present study, some recommendations can be provided.

- No gauging stations are yet installed in the lower part of the Fincha'a watershed, while some of them are installed in the upper part (Figure 4). For the future, greater efforts are needed to install stations evenly distributed in the watershed, aiming to obtain a better monitoring network, which can be used for inferring basin-wide information on the hydro-meteorological dynamics.
- At this moment, there is a reduced agreement on the watershed delineation. In fact, for defining the basin borders, some researchers used the outlet of the Chomen Lake, while others prefer the right bank of the Abbay River. This can result in dissimilarities and uncertainties between the results of studies like the one presented here, and foster a debate among researchers. To solve the situation, the Abbay Basin Authority office should give a clear description of watershed delineation, support decisions and updating information by re-organizing the management information system.
- The great expansion of cultivated land exposes the local community to cutting trees for fuel, construction of timber and generation of additional income, but negatively affecting the natural environment. However, it could be better to wisely use the natural resources, managing them in an integrated, participatory, equitable and sustainable manner.
- If the past trends in LULCC will persist in the future, the observed increase in surface runoff and peak events, as well as soil erosion, could be eventually fostered by climate change, with unforeseen consequences on the local livelihood [28]. Therefore, there is the need for further research, accounting for not only the most up-to-date climate scenarios but also the interrelationship between the natural and the built environment.

Author Contributions: Conceptualization, U.K. and D.A; writing-original draft preparation, U.K., D.A., and M.N; literature review, U.K., D.A. and M.S.R.; modelling, U.K.; supervision, D.A. and M.N..; project administration, D.A.; funding acquisition, M.N. All authors have read and agreed to the published version of the manuscript.

Acknowledgements: The Wollega University is greatly acknowledged for the opportunity to conduct this research. The work of M.N. was supported within statutory activities No. 3841/E-41/S/2021 of the Ministry of Science and Higher Education of Poland. The work of M.S.R. was supported by the NCN National Science Centre Poland–call PRELUDIUM BIS-1, Grant Number 2019/35/O/ST10/00167, project website: https://sites.google.com/view/lulc-fincha/home.

Conflicts of Interest: The authors declare no conflict of interest.

References

1. Githui, F.; Mutua, F.; Bauwens, W. Estimating the impacts of land cover change on runoff using the soil and water assessment tool (SWAT): Case study of Nzoia catchment, Kenya. *Hydrol. Sci. J.* **2010**, 54, 899–908.
2. Calder, C. Hydrologic effects of land use change. In Maidment, D.R. (Ed). *Handbook of Hydrology* **1993**. Eds. McGraw - Hill, New York
3. Alam, A.; Bhat, M.S.; Maheen, M. Using Landsat satellite data for assessing the land use and land cover change in Kashmir valley. *GeoJournal* **2020**, 85(6), 1529-1543.
4. Leta, M.K.; Demissie, T.A.; Tränckner, J. Modeling and Prediction of Land Use Land Cover Change Dynamics Based on Land Change Modeler (LCM) in Nashe Watershed, Upper Blue Nile Basin, Ethiopia. *Sustainability* **2021**, 13(7), 3740.
5. Regasa, M.S.; Nones, M.; Adeba, D. A Review on Land Use and Land Cover Change in Ethiopian Basins. *Land* **2021**, 10, 585
6. Dwivedi, R.S.; Sreenivas, K.; Ramana, K.V. Cover: Land-use/land-cover change analysis in part of Ethiopia using Landsat Thematic Mapper data. *International Journal of Remote Sensing* **2005**, 26(7), 1285-1287.
7. Meyer, W.B; Turner, B.L.II Change in land use and land cover: A Global Perspective. Eds Cambridge: Cambridge University Press 1994, 537 p.
8. Anderson, J.H. A Land Use and Land Cover Classification System for use with Remote Sensor Data. *Geological Survey Professional Paper* **1976**, No. 964.

9. Zhang, L.; Nan, Z.; Yu, W.; Ge, Y. Hydrological responses to land-use change scenarios under constant and changed climatic conditions. *Environmental Management* **2016**, 57(2), 412-431.
10. Negese, A. Impacts of Land Use and Land Cover Change on Soil Erosion and Hydrological Responses in Ethiopia. *Applied and Environmental Soil Science* **2021**. In press.
11. Worku, T.; Khare, D.; Tripathi, S.K. Modeling runoff–sediment response to land use/land cover changes using integrated GIS and SWAT model in the Beressa watershed. *Environmental Earth Sciences* **2017**, 76(16), 1-14.
12. Moriasi, D.N.; Arnold, J.G.; Van Liew, M.W.; Bingner, R.L.; Harmel, R.D.; Veith, T.L. Model evaluation guidelines for systematic quantification of accuracy in watershed simulations. *Transactions of the ASABE* **2007**, 50(3), 885-900.
13. Leta, M.K.; Demissie, T.A.; Koriche, S.A. Impacts of Land Use Land Cover Change on Sediment Yield and Stream Flow: A Case of Finchaa Hydropower Reservoir, Ethiopia. *International Journal of Science and Technology* **2017**, 6(4), 763-781.
14. Berihun, M.L.; Tsunekawa, A.; Haregeweyn, N.; Meshesha, D.T.; Adgo, E.; Tsubo, M.; Masunaga, T.; Fenta, A.A.; Sultan, D.; Yibeltal M.; Ebabu, K. Hydrological responses to land use/land cover change and climate variability in contrasting agro-ecological environments of the Upper Blue Nile basin, Ethiopia. *Science of the Total Environment* **2019**, 689, 347-365.
15. Warburton, M.L.; Schulze, R.E., Jewitt, G.P. Hydrological impacts of land use change in three diverse South African catchments. *Journal of Hydrology* **2012**, 414, 118-135.
16. Bezuayehu, T. People and dams: Environmental and socio-economic impact Fincha'a Hydropower dam, western Ethiopia. *Tropical Res. Manag.* **2006**, 75**.**
17. Makin, M.K. Prospects for Irrigation Development around Lake Ziway, Ethiopia. *Land Resources Study Division* **1976**, Ministry of Overseas.
18. Natural Resources Conservation Service, & Agriculture Department (Eds.). Keys to soil taxonomy. *Government Printing Office*, **2010**.
19. Gyanesh, Ch.; Brian, L.M.; Dennis, L.H. Summary of current radiometric calibration coefficients for Landsat MSS, TM, ETM+, and EO–1 ALI sensors. Remote Sensing of Environment 2009, 113, 893-903.
20. Bezuayehu, T.; Sterk. G. Land use changes induced by a hydropower Reservoir in Fincha'a watershed, western Ethiopia. *Mt. Res. Dev.* **2008**, 28(1),72–80.
21. Taye, H. Dynamics of land use land cover changes on stream flow in Fincha Amerti Neshe sub-basin. Master Thesis, School of Graduate Studies of Addis Abeba University, Ethiopia, **2016**.
22. Campbell, W.G.; Mortenson, D.C. Ensuring the quality of geographic information System data: a practical application of quality control. *Photogrammetric Engineering and Remote Sensing* **1989**, 55, 1613-1618.
23. Setegn, S.G.; Srinivasan, R.; Dargahi, B.; Melesse, A. M. (2009). Spatial delineation of soil erosion vulnerability in the Lake Tana Basin, Ethiopia. *Hydrological Processes: An International Journal* **2009**, 23(26), 3738-3750.
24. Danuso, F. A Stochastic Model for weather data generation. *Italian Journal of Agronomy* **2002**, 6(1), 57-72
25. Arnold, J.G.; Srinivasan, R.; Muttiah, R.R.; Williams, J.R. (1998). Large Area Hydrologic Modeling and Assessment Part I: Model Develop. *Journal of the American Water Resources Association* **1998**, 34(1), 73- 89.
26. Da Silva, M.G.; de Aguiar Netto, A.D.O.; de Jesus Neves, R.J.; Do Vasco, A.N.; Almeida, C.; Faccioli, G.G. (2015). Sensitivity analysis and calibration of hydrological modeling of the watershed Northeast Brazil. *Journal of Environmental Protection* **2015**, 6(08), 837.
27. Kumar, S.; Mishra, A. Critical erosion area identification based on hydrological response unit level for effective sedimentation control in a river basin. *Water Resources Management* **2015**, 29(6), 1749-1765.
28. Dibaba, W.T.; Demissie, T.A.; Miegel, K. Prioritization of Sub-Watersheds to Sediment Yield and Evaluation of Best Management Practices in Highland Ethiopia, Finchaa Catchment. *Land* **2021**, 10, 650.